Journal of Photochemistry and Photobiology A: Chemistry 201 (2009) 32–38

Contents lists available at ScienceDirect

Journal of Photochemistry and Photobiology A: Chemistry

journal homepage: www.elsevier.com/locate/jphotochem

Effect of simulated solar light on the autocatalytic degradation of nitrobenzene using Fe^{3+} and hydrogen peroxide

Luciano Carlos[a], Debora Fabbri[b], Alberto L. Capparelli[a], Alessandra Bianco Prevot[b], Edmondo Pramauro[b], Fernando García Einschlag[a,*]

[a] Instituto de Investigaciones Fisicoquímicas Teóricas y Aplicadas (INIFTA), CCT-La Plata-CONICET, Departamento de Química, Facultad de Ciencias Exactas, Universidad Nacional de La Plata (UNLP), Diagonal 113 y 64, Casilla de Correo 16, Sucursal 4, Código Postal 1900, La Plata, Argentina
[b] Dipartimento di Chimica Analitica, Università di Torino, Italy

ARTICLE INFO

Article history:
Received 16 April 2008
Received in revised form 19 August 2008
Accepted 19 September 2008
Available online 4 October 2008

Keywords:
Photo-Fenton
Solarbox
Nitroaromatic
Autocatalysis

ABSTRACT

The effect of simulated solar light on nitrobenzene degradation in Fe^{3+}/H_2O_2 solutions was investigated under different experimental conditions. Consumption profiles of NBE and H_2O_2 display an autocatalytic kinetic behavior for both dark and photo-assisted degradation experiments. The rates of the initial slow phase that precedes the catalytic phase are significantly enhanced by irradiation, although the effect of simulated solar light on the rates of the fast phase is negligible. The absolute rates of the slow phase increase with the concentrations of Fe^{3+} and H_2O_2, whereas the initial rate of the degree of conversion increase decreases with organic matter loading. The reaction progress was characterized by HPLC, GC–MS, IC, TOC (total organic carbon) and toxicity analyses. The main products detected were 4-nitrophenol, 3-nitrophenol, 2-nitrophenol, 1,3-dinitrobenzene, phenol, oxalic acid, formic acid, NO_2^- and NO_3^-. Product distribution profiles are discussed in connection with TOC and toxicity measurements. The results show that dark treatment is neither capable of lowering the organic content nor capable of reducing the effluent toxicity to acceptable levels. On the other hand, photo-assisted processes induced by simulated solar light can significantly enhance both mineralization and detoxification efficiencies.

1. Introduction

Photochemical remediation of wastewater using solar radiation is an active research field in modern environmental science. Although biological treatment is broadly applied to the treatment of wastewater from urban areas, a large number of compounds are not biodegradable due to their high toxicity. Therefore, alternative or additional methods for detoxification are of current interest.

In recent years, increasing attention has been focused on the Advanced Oxidation Technologies (AOTs), especially those capable of using solar radiation, since they have proved to be efficient for the degradation and eventual mineralization of refractory contaminants [1–5]. One of the most promising AOTs is the photo-assisted oxidation of organic pollutants in aqueous solution by hydrogen peroxide and catalytic amounts of iron salts, i.e., the photo-Fenton technique. This process has a number of advantages: (i) iron is non-toxic and abundant in nature; (ii) the reagents used are safe to handle and environmentally benign; (iii) the oxidation can be very efficient under mild operating conditions including room temperature and atmospheric pressure; (iv) there are no mass transfer limitations due to its homogeneous catalytic nature. In addition, the use of solar radiation can considerably reduce the operating costs making it a feasible technology to be applied directly from laboratory to plant scale [6].

Although the reaction manifold involved in the mineralization process can be quite complex, it is generally accepted that the oxidation of organic substrates (S) in Fenton systems is related to the highly efficient generation of hydroxyl radicals during H_2O_2 decomposition by Fe^{2+} in acidic medium ((R1) and (R2)) [7,8]:

$$Fe^{2+} + H_2O_2 \rightarrow Fe^{3+} + HO^\bullet + HO^- \quad (R1)$$

$$S + HO^\bullet \rightarrow Oxid.Prod. \quad (R2)$$

In photo-Fenton systems, the positive effect of irradiation is mainly related to the photoreduction of $Fe(OH)^{2+}$ (R3), the dominant ferric species in the pH range between 2 and 3, to yield hydroxyl radicals and Fe^{2+} that can further react with H_2O_2:

$$Fe(OH)^{2+} + h\nu \rightarrow Fe^{2+} + HO^\bullet \quad (R3)$$

Under the conditions commonly used in photo-Fenton systems, reactions (R1) and (R2) readily take place, the overall rate

* Corresponding author. Tel.: +54 221 425 7291/425 7430; fax: +54 221 425 4642.
E-mail address: fgarciae@quimica.unlp.edu.ar (F. García Einschlag).

1010-6030/$ – see front matter © 2008 Elsevier B.V. All rights reserved.
doi:10.1016/j.jphotochem.2008.09.012

of substrate degradation being mainly controlled by the rate of Fe^{2+} production. In addition, if used at rather high concentrations, hydrogen peroxide can act as a scavenger of hydroxyl radicals (R4), thus diminishing the efficiency of the substrate degradation:

$$H_2O_2 + HO^\bullet \rightarrow HO_2^\bullet + H_2O \quad (R4)$$

Nitroaromatic compounds are extensively used as raw materials in many industrial processes such as in the preparation of pesticides, explosives, dyes, pulp and paper. The detoxification of wastewaters containing these compounds is very difficult since, due to their high stability, they are usually refractory to biological degradation [9]. Several studies have addressed the use of photo-Fenton technique for the destruction of nitroaromatic compounds [10–13]; however, some aspects concerning the relative contribution of thermal and photochemical reaction steps in $Fe^{3+}/H_2O_2/h\nu$ systems to the mineralization and detoxification processes have not been completely clarified. Thus we focused our study on the kinetics of Fenton-like and solar-Fenton processes that use catalytic amounts of ferric salts. It is worth mentioning that the degradation aromatic substrates in H_2O_2/Fe^{3+} systems frequently display autocatalytic concentration profiles with an initial slow phase followed by a catalytic phase [14,15]. Since the initial reaction rates are much slower than those associated with the catalytic phase, the overall efficiency is governed by the extent of the initial slow phase. Moreover, it has been shown that in Fenton-like systems, both the extent of the slow phase and the difference between the rates observed in each phase increase with increasing substrate concentration and decreasing catalyst concentration [16].

In this work, we studied the autocatalytic degradation of nitrobenzene (NBE) in Fe^{3+}/H_2O_2/UV–vis systems at low catalyst concentrations. In order to assess the relative contributions of thermal and photochemical pathways, we compared the NBE and H_2O_2 concentration profiles observed in the absence and in the presence of simulated solar light. The effect of initial reagent concentrations on the consumption rates of NBE and H_2O_2 associated with each reaction phase was also investigated. In addition, the evolution of the reaction mixture composition and the detoxification efficiency (characterized by HPLC, GC–MS, IC, TOC (total organic carbon) and toxicity bioassays) are discussed in detail.

2. Materials and methods

2.1. Reagents

Nitrobenzene (Fluka), 1,3-dinitrobenzene (Merk), 2-nitrophenol (Riedel de Haën), 3-nitrophenol (Riedel de Haën), 4-nitrophenol (Riedel de Haën), phenol (Sigma–Aldrich), 4-nitrocatechol (Aldrich), hydroquinone (Fluka), 1,4-benzoquinone (Fluka), catechol (Merck), H_2O_2 (Merck), $Fe(ClO_4)_3{\cdot}nH_2O$ (Aldrich), $K_2C_2O_4{\cdot}H_2O$ (Merk), $NaNO_2$ (Carlo Erba), KNO_3 (Carlo Erba) and formic acid (Carlo Erba) of analytical grade were used as received.

Nitrohydroquinone and 3-nitrocatechol were prepared by hydroquinone and catechol nitration, respectively, using $NaNO_2$ in acid medium according to the method described elsewhere [17].

2.2. Analytical techniques

2.2.1. HPLC

The concentration profiles of NBE and several aromatic products were tracked using Merck-Hitachi equipment (pump L-6200, UV-Vis detector L-4200). An RP-C18 column (Lichrospher, 4 mm i.d. × 12.5 mm length) was used with the following elution conditions: mobile phase composed of 30/70 (v/v) acetonitrile and an aqueous solution ($[H_3PO_4] = 0.01\ mol\ L^{-1}$ and [triethylamine] = 0.01 mol L^{-1}, pH 3.0); flow rate: 1 mL min^{-1} and detection wavelength 220 nm. In order to prevent the decomposition of organic components prior to the HPLC analysis, 1 mL samples withdrawn from the reactor were immediately mixed with 0.3 mL of methanol.

2.2.2. GC–MS

The reaction products were analyzed using a gas chromatograph (Varian 3400) coupled to an ionic trap mass spectra detector (Varian Saturn 4D) and equipped with a capillary column (Supelco, Fused Silica Capillary, 0.25 mm i.d. and 30 m length). Column temperature: 60 °C for 1 min, up to 300 °C (ramp of 15 °C min^{-1}) and constant for 1 min. The temperature of the injection port was 250 °C and the injection volume was 1 μL. Reaction products were identified by comparison of their retention times and mass spectra with the corresponding standards. Prior to the analysis, the samples (4 mL) were extracted twice with 8 mL of tertbutylmethylether; the collected organic phase was reduced to a volume of 1 mL under N_2 flow at room temperature.

2.2.3. IC

Low-molecular-weight organic acids and inorganic anions were identified by ionic chromatography using a Dionex DX-500 instrument, equipped with a Dionex column (AS9-HC, 200 mm length and 4 mm i.d.), an electrochemical detector (ED40) and a gradient pump (GP40). Mobile phase: $[K_2CO_3] = 9\ mmol\ L^{-1}$. Flow rate: 1.5 mL min^{-1}. Iron was eliminated prior to the analysis by adding NaOH until pH 7.0 and subsequently filtering through nylon filters (0.22 μm).

2.2.4. TOC

The evolution of TOC was monitored using Shimadzu equipment (5000 TOC analyzer, catalytic oxidation on Pt at 680 °C).

2.2.5. H_2O_2

Hydrogen peroxide concentration profiles were measured by means of an enzymatic-colorimetric method, using a mixture of phenol (0.025 mol L^{-1}), 4-aminoantipyrine (5×10^{-3} mol L^{-1}), phosphate buffer (pH 6.9) and peroxidase (10 mg L^{-1}) [18]. In the presence of H_2O_2 a quinoneimine with an absorption maximum at 510 nm is formed. Aliquots of 0.1 mL of the reaction mixture were added to 2 mL of colorimetric reagent, the absorbance was recorded after 1 min of incubation at room temperature.

2.3. Toxicity assays

The toxicity evolution of irradiated and nonirradiated samples was studied using a Microtox 500 analyzer (Strategic Diagnostics Inc.). The bioluminescence of the marine bacterium *Vibrio fisheri* was used to evaluate the toxicity of the samples. Since this bacterium emits light as a result of its normal metabolism ($\lambda_{Em,Max}$ 490 nm), the reduction of the emission intensity is a measure of the sample toxicity (i.e., the presence of substances that interfere with normal metabolic activity).

The reduction of the bioluminescence was evaluated for several sample dilutions through measurements after 5 min of contact time. From a statistical analysis of the data, the effective concentrations that reduced the bioluminescence intensity (EC_{50}) by 50% were calculated. Using the EC_{50} values, the toxicity units (TU) associated with each sample were obtained by means of the following expression:

$$TU = \frac{100}{EC_{50}} \quad (1)$$

In addition, detoxification efficiencies (DE%), calculated from TU values of treated (TU_f) and untreated (TU_i) samples, were used for

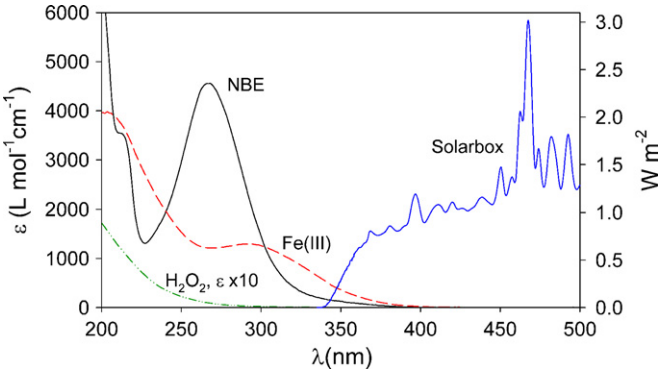

Fig. 1. Irradiance spectra of the Solarbox (equipped with a 340 nm cutoff filter); molar absorption coefficients of H_2O_2, NBE and $FeClO_4$ at pH 3.0.

comparison purposes:

$$DE\,(\%) = \frac{TU_i - TU_f}{TU_i} \times 100 \quad (2)$$

In order to eliminate the effects of pH and Fe^{3+} on TU values, samples were neutralized and iron was eliminated by filtration prior to the toxicity analysis. No significant differences between the measured toxicities were observed in the absence or in the presence of H_2O_2. All bioassays were conducted following the standard Microtox protocol, and data analysis was performed using the Microtox Omni Software.

2.4. Experimental conditions

The experiments were carried out in a cylindrical Pyrex cell (40 mm i.d. × 25 mm height) at 25 °C and under continuous stirring. A 1500 W xenon lamp (Solarbox, CO. FO. MEGRA, Milan, Italy) equipped with a cutoff filter of 340 nm was used. The measured photonic flux of the simulated AM1 radiation (wavelength range: 340–400 nm) was ca. 1.4×10^{-5} Einsteins min^{-1} in the reactor cell [19]. The resulting emission spectra and the absorption spectra of the reagents are shown in Fig. 1.

Working solutions were prepared daily with water of milli-Q quality, $HClO_4$ was used to adjust the pH to 3.0 since ClO_4^- is a noncomplexing and nonreacting anion [20]. Concentrations of NBE, Fe^{3+} and H_2O_2 were in the ranges 0.3–1 mmol L^{-1}, 0.01–0.2 mmol L^{-1} and 2.3–17 mmol L^{-1}, respectively.

3. Results and discussion

3.1. Effect of the irradiation

Blank experiments carried out by irradiating NBE solutions using the Solarbox in the absence of H_2O_2 and Fe(III) showed a negligible degradation of the substrate in the spanned timescale. Comparative NBE degradation tests were conducted in the dark and under continuous irradiation; for this set of tests besides the 340 nm cutoff filter an additional 300 nm cutoff filter was used. The normalized concentration profiles of NBE and H_2O_2 display an autocatalytic behavior (Fig. 2); an initial "slow phase" is followed by a "fast phase" where the consumption rates of both NBE and H_2O_2 are substantially increased. It is important to notice that NBE profiles show the transition from the slow phase to the fast phase for conversion degrees lower than 15% (Fig. 2A).

Previous studies of NBE degradation in the absence of radiation [21] have shown that the autocatalytic behavior is correlated with the existence of two pathways of Fe^{2+} production. At early elapsed times, the rate of Fe^{2+} generation is controlled by the slow thermal

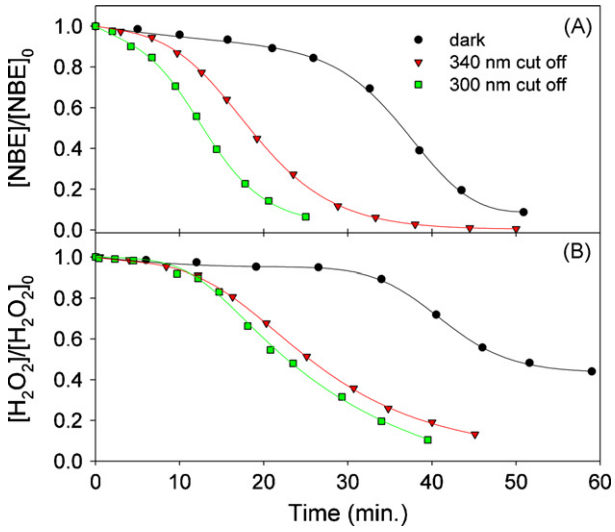

Fig. 2. Effect of irradiation on kinetic profiles: (A) NBE and (B) H_2O_2. Initial concentrations: $[NBE]_0 = 1$ mmol L^{-1}, $[Fe^{3+}]_0 = 0.86$ mmol L^{-1} and $[H_2O_2]_0 = 7.7$ mmol L^{-1}.

reduction of Fe^{3+} by H_2O_2 (R5):

$$Fe^{3+} + H_2O_2 \rightarrow Fe^{2+} + HO_2^{\bullet} + H^+ \quad (R5)$$

By the end of the induction period, hydroxylated products able to reduce Fe^{3+} (i.e., *ortho*- and *para*-dihydroxybenzene derivatives ($DHBH_2$)) are accumulated in the reaction mixture, thus promoting a second pathway for Fe^{2+} production (R6) [15,22]:

$$Fe^{3+} + DHBH_2 \rightarrow Fe^{2+} + DHBH^{\bullet} + H^+ \quad (R6a)$$

$$Fe^{3+} + DHBH^{\bullet} \rightarrow Fe^{2+} + DHB + H^+ \quad (R6b)$$

Fig. 2 shows that the induction period preceding the catalytic phase is significantly shortened in the presence of radiation. Since the photolysis of hydrogen peroxide by solar irradiation can be neglected (Fig. 1), this behavior can be explained by considering the photo-assisted reduction of Fe^{3+} species to yield Fe^{2+} and hydroxyl radicals ($HO^{\bullet}$) (R3). The comparison of the concentration profiles obtained for dark and irradiated experiments shows that the initial NBE degradation rates, which were calculated from the slope of the curves, increase by a factor of 2 with $\lambda \geq 340$ nm and by a factor of 4 with $\lambda \geq 300$ nm. These results indicate an important contribution of the photochemical pathways during the initial oxidation stages. As a result, the time required for the accumulation of dihydroxybenzene derivatives closely related to the catalytic phase is largely reduced by irradiation.

Unlike the slow phase, NBE consumption rates observed during the fast phase for the experiments conducted in the dark and under irradiation with different sources are very similar (i.e., dark and 340 nm cutoff experiments yielded almost the same value, whereas the rate observed for the 300 nm cutoff experiment does not differ by more than 20%). These results suggest that photochemical reactions induced by $\lambda > 340$ nm have a negligible contribution to the fast phase kinetics and that the observed catalysis is mainly governed by thermal reduction of Fe^{3+} species due to aromatic intermediates (R6).

It is important to notice here that, even though during the dark experiment only a 10% of NBE is consumed in the initial phase, this period encompasses more than 50% of the time required for complete NBE oxidation (Fig. 2A). Thus, the technical significance of the use of irradiation in autocatalytic Fenton systems is mainly related to the shortening of the slow phase. Another relevant issue is that the fraction of H_2O_2 consumed in the dark experiment is only 60%, whereas an almost complete consumption of hydrogen

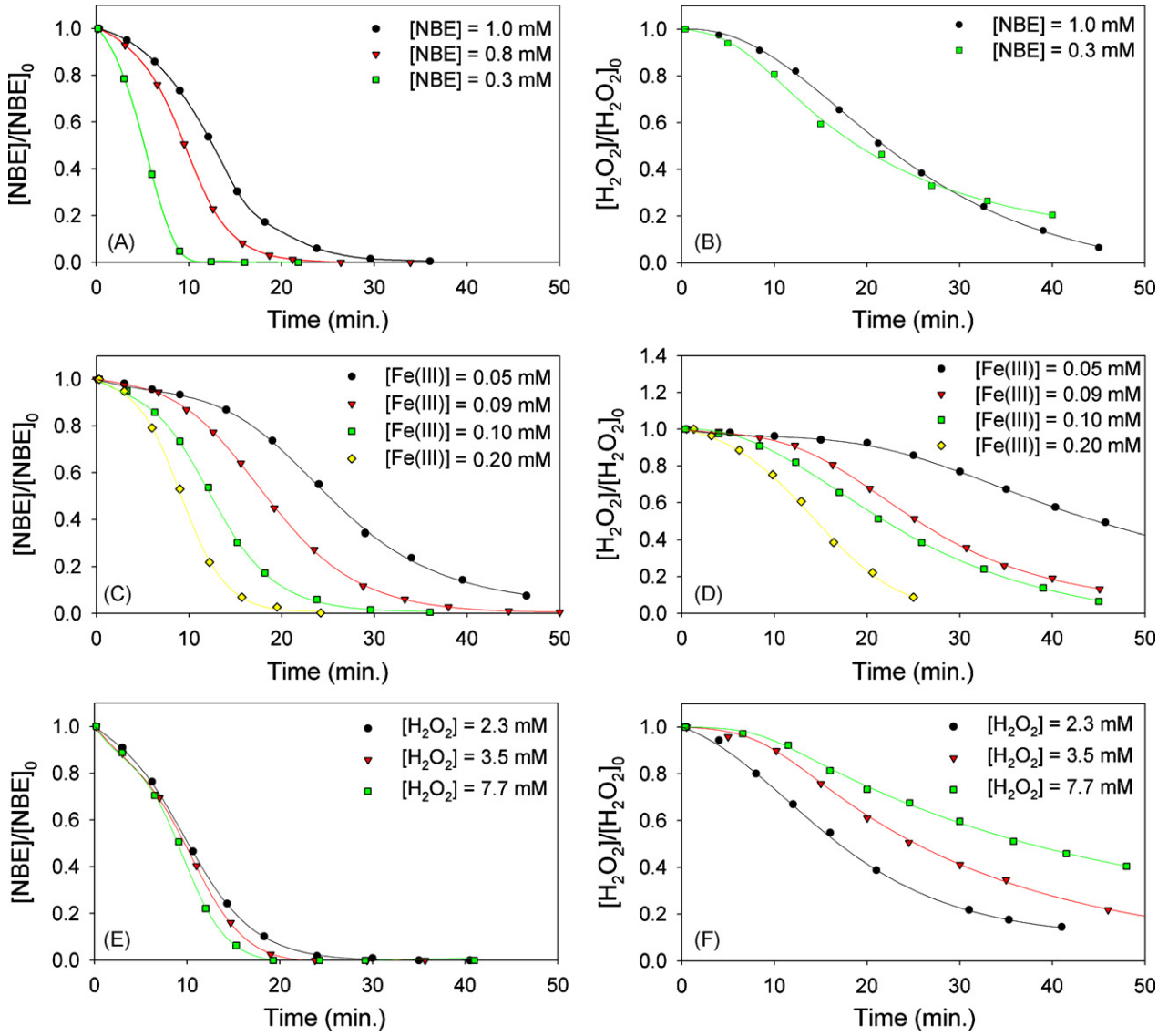

Fig. 3. Effect of initial reagent concentrations on normalized NBE and H_2O_2 kinetic profiles obtained under simulated solar light. (A and B) $[Fe^{3+}]_0 = 0.1$ mmol L^{-1} and $[H_2O_2]_0 = 7.7$ mmol L^{-1}. (C and D) $[NBE]_0 = 1$ mmol L^{-1} and $[H_2O_2]_0 = 7.7$ mmol L^{-1}. (E and F) $[NBE]_0 = 0.3$ mmol L^{-1} and $[Fe^{3+}]_0 = 0.05$ mmol L^{-1}.

peroxide is observed for the irradiated solutions. This result will be discussed below (Section 3.4).

3.2. Effect of initial concentrations

Fig. 3 shows the effects of the initial reagent concentrations on the kinetic behavior of both NBE and H_2O_2 observed for irradiated samples. The relative standard error, determined on at least five replicated runs for selected measurements, was lower than 2% for NBE and lower than 4% for H_2O_2. In order to compare the autocatalytic profiles, the transition between the slow phase and the fast phase was assumed to occur at a 10% NBE conversion degree [16,23]. The estimations of the average consumption rates, before (r^{NBE}_{Slow} and $r^{H_2O_2}_{Slow}$) and after (r^{NBE}_{Fast} and $r^{H_2O_2}_{Fast}$) the transition, are shown in the supplementary information as in Table S1.

3.2.1. Organic matter loading

Fig. 3A and B shows the kinetic profiles observed for NBE and H_2O_2 using different initial concentrations of organic matter; for comparison purposes normalized concentrations are depicted. The estimated average consumption rates (Exp. 1–3, Table S1) show that the increase in $[NBE]_0$ increases r^{NBE}_{Slow} by 20%, decreases $r^{H_2O_2}_{Slow}$ by 19% and significantly delays the transition times to the fast phase. It should also be noted that r^{NBE}_{Slow} does not depend linearly on [NBE] since an increase of [NBE] by a factor of 3 produces an increase of only 20% in r^{NBE}_{Slow}. Thus, although r^{NBE}_{Slow} increases with $[NBE]_0$, the initial slopes of the normalized NBE profiles (given by $r^{NBE}_{Slow}/[NBE]_0$) decrease with increasing organic matter concentration.

Considering that the NBE degradation rate is proportional to both NBE and HO• concentrations (i.e., $r_{R2} = -d[NBE]/dt = k_{NBE}\cdot[HO^\bullet]\cdot[NBE]$), these results indicate that increasing NBE concentration decreases the steady-state concentration of hydroxyl radicals ($[HO^\bullet]_{ss}$). The decrease in $[HO^\bullet]_{ss}$ can be explained taking into account that high concentrations of organic matter decrease the fraction of photons absorbed by Fe^{3+} species due to an inner filter effect and also decrease HO• lifetime due to a scavenging effect. A brief discussion of both effects is given in the following sections.

3.2.1.1. Inner filter effect. Using the absorption spectra of NBE and Fe^{3+} shown in Fig. 1, we estimated the initial fractions of photons absorbed by Fe^{3+}($\alpha_{Fe^{3+}}$) under different experimental conditions:

$$\alpha_{Fe^{3+}} = \frac{1}{n_\lambda}\sum_{\lambda=340}^{400}\frac{\varepsilon^{\lambda}_{Fe^{3+}}[Fe^{3+}]}{\varepsilon^{\lambda}_{Fe^{3+}}[Fe^{3+}] + \varepsilon^{\lambda}_{NBE}[NBE]} \quad (3)$$

The results obtained for the wavelength range 340–400 nm show that the fraction of radiation absorbed by Fe^{3+} diminishes from around 45% to 22% when $[NBE]_0$ is increased from 0.3 mmol L^{-1} to 1 mmol L^{-1}. Hence, the contribution of the photochemical reduction of Fe^{3+} to the initial rates is considerably diminished for high concentrations of organic matter.

3.2.1.2. Scavenging effect. During the initial stages of the oxidation process, thermal and photochemically produced hydroxyl radicals react almost exclusively with NBE and H_2O_2 ((R2) and (R4)). Hence, we used known rate constant values [24] to estimate the HO• half-life ($t1/2$) and the fraction of HO• scavenged by NBE (σ_{NBE}):

$$t1/2 = \frac{\ln(2)}{k_{NBE}[NBE] + k_{H_2O_2}[H_2O_2]} \quad (4)$$

$$\sigma_{NBE} = \frac{k_{NBE}[NBE]}{k_{NBE}[NBE] + k_{H_2O_2}[H_2O_2]} \quad (5)$$

As $[NBE]_0$ is increased, the computed lifetimes decrease from 0.43 μs to 0.15 μs, whereas the fractions scavenged by NBE increase from 0.83 to 0.94.

Finally, since conversion degrees near 10–15% are required for the beginning of the catalytic phase, the increase of the transition time with $[NBE]_0$ is closely related to the decrease of the initial rate of the degree of conversion increase (i.e., $r^{NBE}_{Slow}/[NBE]_0$).

Concerning hydrogen peroxide behavior during the slow phase, the aforementioned inner filter and scavenging effects also account for the decrease in $r^{H_2O_2}_{Slow}$ with $[NBE]_0$. The increase of NBE concentration causes a decrease in Fe^{2+} photoproduction rate and also decreases the fraction of HO• available to react with hydrogen peroxide (R4).

In relation to the fast phase, a small increase of r^{NBE}_{Fast} values is observed with the increase of $[NBE]_0$, thus a higher organic matter loading does not produce a significant effect on the overall degradation rates. In addition, it should be pointed out that H_2O_2 consumption rates do not show a significant dependence on the initial NBE concentration. Taking into account that hydrogen peroxide is mainly consumed through (R1), this suggests that average $[Fe^{2+}]$ during the fast phase is practically independent of $[NBE]_0$ and further supports that the contribution of photochemical processes to Fe^{3+} reduction is of minor importance during the fast phase. These results are in agreement with those presented in Section 3.1.

Taking into account the results discussed above, it is clear that an important parameter in photo-Fenton systems is the initial concentration of organic matter, since aromatic compounds can strongly influence the kinetics of the process due to both inner filter and scavenging effects.

3.2.2. Effect of initial [Fe^{3+}]

The effect of the initial Fe^{3+} concentration on the degradation kinetics is presented in Fig. 3C and D (Exp. 4–7, Table S1). As expected, the transformation rates of NBE and H_2O_2 during both phases substantially increase with catalyst concentration. Since the kinetic profiles are controlled by Fe^{2+} production, an increase in $[Fe^{3+}]_0$ results in faster degradation and shorter transition times due to the enhancement of Fe^{3+} reduction rates through reactions (R3), (R5) and (R6).

3.2.3. Effect of initial [H_2O_2]

The concentration profiles of NBE are only slightly dependent on $[H_2O_2]_0$ under the tested conditions (Fig. 3E). The relatively small effect of hydrogen peroxide on the degradation rates indicates that H_2O_2 does not participate (at least directly) in the rate-controlling steps of the overall process. The analysis of H_2O_2 concentration profiles (Fig. 3F) shows that the excess of oxidant, available for further mineralization steps, observed after complete NBE consumption increases with $[H_2O_2]_0$.

3.3. Analysis of aromatic products

The distributions of aromatic NBE byproducts, corresponding to different conversion degrees, were studied using HPLC and GC–MS analyses. In both dark and irradiated experiments, the same products were detected: 2-nitrofenol, 3-nitrofenol, 4-nitrofenol, phenol, 1,3-dinitrobenzene, 4-nitrocatechol, 3-nitrocatechol, nitrohydroquinone, benzoquinone, catechol, 1,2-dinitrobenzene and 1,4-dinitrobenzene. The kinetic profiles (Fig. S1 in supplementary information) were used to evaluate the primary yields of nitrophenolic products as described in a recent paper [17]. Although shorter timescales and higher absolute yields were observed for the irradiated samples, the relative distributions of nitrophenol isomers were similar in the presence and in the absence of irradiation (see η^N values of Table S2, supplementary information). Thus, during the degradation stages that involve aromatic byproducts, irradiation mainly plays a kinetic role by accelerating the overall reaction rates, although its mechanistic effect is less pronounced because the relative product distributions are not affected.

Among the detected byproducts, 4-nitrocatechol, 3-nitrocatechol, nitrohydroquinone and catechol contain two HO groups in relative *ortho*- or *para*-positions. Hence, the observed autocatalysis could be related to the formation of these compounds since they would be able to reduce Fe^{3+} [22].

It is worth mentioning that, with the exception of 1,3-dinitrobenzene, only traces of aromatic compounds are detected after 50 min (irradiated experiment) or 70 min (dark experiment). These are important results because aromatic compounds are usually more hazardous than their corresponding aliphatic oxidation products [25]. However, attention should be paid to 1,3-dinitrobenzene since due to its low reactivity towards hydroxyl radicals it may require longer reaction times for its complete depletion.

3.4. Ion chromatography analysis

The concentration profiles of NO_2^-, NO_3^-, formic acid and oxalic acid were followed by IC. Fig. 4 compares the kinetic curves obtained in the dark (A) and under irradiation (B). The reported IC results were obtained from single injections; therefore, the corresponding error was not evaluated. In agreement with NBE and H_2O_2 concentration profiles, IC chromatograms show an earlier formation of products for the irradiated samples.

For both dark and irradiated samples small amounts of NO_2^-, consistent with phenol detection among primary NBE degradation products [17], are found before the catalytic phase begins. However, the highest NO_2^- concentrations are reached after NBE conversion degrees higher than 70%, suggesting that intermediate products also release NO_2^- during their decomposition. On the other hand, the highest NO_3^- production rates are coincident with the apexes of NO_2^- profiles, indicating that NO_3^- is formed from NO_2^- due to the oxidizing conditions of the reaction mixture.

It is worth noting that carboxylic acid profiles show significant differences. While oxalic and formic acid profiles rise till they reach almost constant values in dark experiments, they show a steep

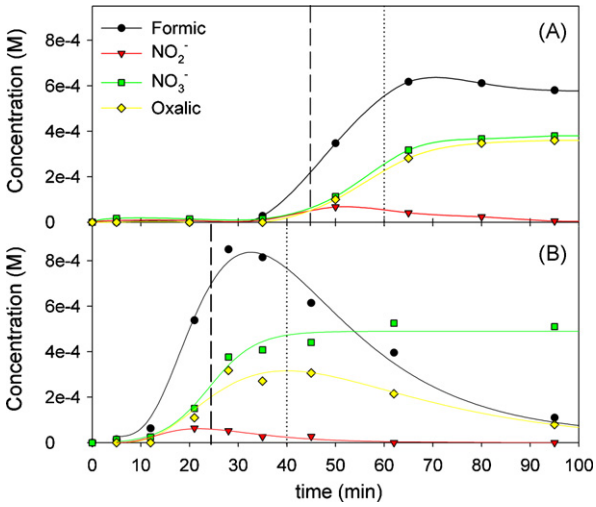

Fig. 4. Comparison of IC profiles obtained in the absence (A) and in the presence (B) of irradiation. $[NBE]_0 = 1\ mmol\ L^{-1}$, $[Fe^{3+}]_0 = 0.1\ mmol\ L^{-1}$ and $[H_2O_2]_0 = 7.7\ mmol\ L^{-1}$. Dash line, 80% NBE conversion degree; dotted line, 95% aromatic byproduct conversion degree.

decrease after their maxima for the irradiated solutions. This behavior can be explained by considering the formation of Fe^{3+} complexes with oxalate and formate anions, given that these species are fairly stable towards hydroxyl radical attack but exhibit high quantum yields of photolysis (R7) [2,26]:

$$Fe(III)(RCO_2)^{2+} + h\nu \rightarrow Fe^{2+} + CO_2 + R^{\bullet} \quad (R7)$$

Under the experimental conditions of the present work, the carboxylic acids produced as the reaction progresses can form strong complexes with ferric ions [27], thus preventing Fe^{3+} thermal reduction mediated by H_2O_2 [28]. The aforementioned complexes are known to absorb a larger fraction of solar radiation than Fe^{3+}-aquo complexes and their photolysis can readily lead to the formation of CO_2 and Fe^{2+}, thus increasing H_2O_2 consumption (Fig. 2B) and yielding additional $HO^{\bullet}$ radicals through Fenton reaction (R1). Hence, in agreement with the previous studies [26], our results confirm a critical contribution of the photolysis of Fe^{3+}–organic acid complexes to the global mineralization mechanism in the presence of radiation.

3.5. TOC analysis

The normalized TOC profiles of Fig. 5 show a very poor mineralization efficiency during the dark experiment, the reduction in the organic matter content being only 5% after 90 min. On the other hand, the irradiated experiment carried out using the same initial reagent concentrations shows a decrease in the organic content larger than 70% at the same timescale. The differences in the TOC profiles are well correlated with the IC analyses (i.e., relatively high and rather constant concentrations of oxalic and formic acids were detected after 90 min of dark treatment, whereas significant decreases were observed for the irradiated samples).

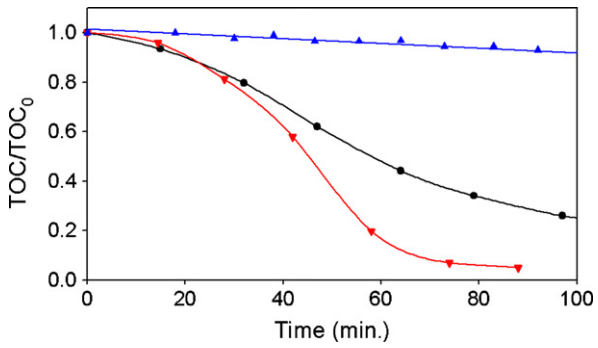

Fig. 5. Comparison of total organic carbon profiles. $[NBE]_0 = 1\ mmol\ L^{-1}$ and $[Fe^{3+}]_0 = 0.1\ mmol\ L^{-1}$. (▲) dark, $[H_2O_2]_0 = 7.7\ mmol\ L^{-1}$; (●) irradiation, $[H_2O_2]_0 = 7.7\ mmol\ L^{-1}$; (▼) irradiation, $[H_2O_2]_0 = 12\ mmol\ L^{-1}$.

In addition, the comparison between the profiles of irradiated samples obtained using different $[H_2O_2]_0$ values shows that increasing the initial additive concentration improves the mineralization efficiency, since a reduction of 94% in the TOC content is achieved after 80 min of irradiation in the experiment performed with higher $[H_2O_2]_0$. These results can be explained taking into account that, in the absence of other oxidants, the minimal concentration of H_2O_2 required for complete mineralization of $1\ mmol\ L^{-1}$ of NBE should be at least $15\ mmol\ L^{-1}$ (i.e., $C_6H_5NO_2 + 15H_2O_2 \rightarrow 6CO_2 + 17H_2O + HNO_3$).

3.6. Toxicity analysis

Toxicity tests on both initial and treated samples were carried out in order to provide a more complete evaluation of the efficiency of the technologies used. TU values and detoxification efficiencies, presented in Table 1, show that the toxicity diminishes only 49% after 75 min of dark treatment, whereas detoxification efficiencies higher than 85% are achieved after 1 h of irradiation. It is also observed that increasing $[H_2O_2]_0$ leads to an improvement of the detoxification process.

Fig. 6 shows the toxicity evolution registered during dark and photo-assisted treatments. The comparison between inhibition percentage and normalized TOC profiles shows similar trends for the irradiated samples; nevertheless, TOC curves cannot be directly correlated with toxicity bioassays for the nonirradiated solutions.

For the dark experiment the inhibition does not decrease throughout the first 50 min, in line with the TOC profile and the high concentrations of reaction intermediates (Sections 3.3 and 3.4). However, although the dissolved organic content remains almost constant after 75 min, a noticeable decrease in the toxicity is observed. This result can be related to the important decrease in the concentration of aromatic compounds, as suggested by HPLC and GC–MS analyses. The remaining toxicity can be explained by considering the residual amounts of 1,3-dinitrobenzene and, probably to a lesser extent, that of nonaromatic compounds.

In the case of the irradiated samples, the important toxicity decrease is accompanied by significant reductions of both byproduct concentrations and total organic carbon. In addition, the

Table 1
Comparison of TU and DE% results.

No.	NBE ($mmol\ L^{-1}$)	Fe^{3+} ($mmol\ L^{-1}$)	H_2O_2 ($mmol\ L^{-1}$)	Condition	TU initial	TU final	DE (%)
1	1	0.1	7.7	Darkness	4.73	2.43[a]	49[a]
2	1	0.1	7.7	Solarbox	4.73	0.67[b]	86[b]
3	1	0.1	12	Solarbox	4.73	0.26[b]	95[b]

[a] 75 min.
[b] 60 min.

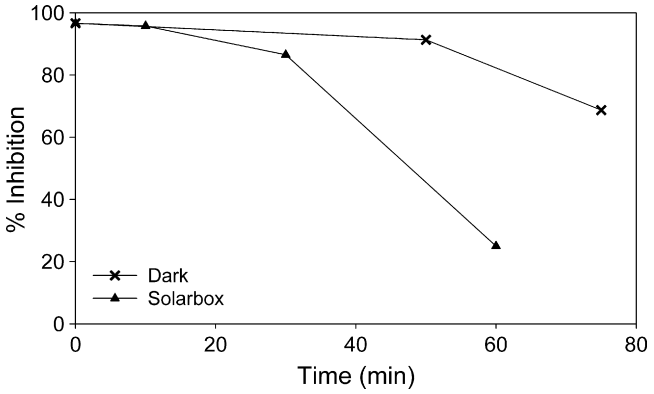

Fig. 6. Toxicity evolution for treated samples in the absence and in the presence of irradiation. $[NBE]_0 = 1$ mmol L^{-1}, $[Fe^{3+}]_0 = 0.1$ mmol L^{-1} and $[H_2O_2]_0 = 7.7$ mmol L^{-1}.

dissimilar DE% values achieved with different $[H_2O_2]$ are in line with the larger mineralization degrees observed in the presence of higher excess of oxidant.

It is important to emphasize that the use of simulated solar light allows attaining higher and faster reductions of toxicity. Furthermore, acceptable DE% values are achieved in the photo-induced processes since solutions with TU levels lower than 1 are considered as nontoxic [29], confirming that simulated solar light plays a fundamental role in the detoxification process.

4. Conclusions

Nitrobenzene degradation by Fe^{3+}/H_2O_2 and Fe^{3+}/H_2O_2/UV–vis treatments displays an autocatalytic behavior. Photo-induced reactions increase the rates associated with the initial slow phase, significantly reducing the transition times and enhancing the overall efficiency. However, the irradiation of the solutions with wavelengths larger than 340 nm has a negligible effect on the rates associated with the catalytic phase. Because the efficiency of the autocatalytic system is limited by the slowness of the initial phase, the use of simulated solar light improves the effectiveness of the overall oxidation through an acceleration of the slow phase.

Since the transition times from the slow to the fast phase increase at high ratios of organic matter concentration with respect to catalyst concentration and the photoreduction of Fe^{3+} species may be hindered by inner filter effects, the [substrate]/[catalyst] ratio is a critical parameter for design purposes.

The results obtained in the absence of irradiation show that toxicity and TOC profiles are not necessarily correlated. Therefore, the interpretation of the temporal evolution of toxicity levels requires the use of complementary analytical techniques. Besides, the use of simulated solar light allows attaining faster and higher reductions of toxicity levels owing to the contribution of additional photochemical pathways ((R3) and (R7)).

The comparative analysis of both reaction rates and product distributions observed for dark and irradiated experiments shows that photo-assisted processes play different roles depending on the reaction stage considered. During the initial slow phase irradiation mainly plays a kinetic role, whereas along the catalytic phase its effect on both the reaction rates and the primary yields is of minor importance. Throughout the final treatment stages, photo-induced processes strongly affect both the overall kinetics and the product distributions since noticeable differences in the shapes of aliphatic acid profiles are observed.

Acknowledgments

This work was supported in part by a project grant from the CONICET (Grant No. PIP6301). Financial support from MIUR (Rome) is gratefully acknowledged. A. Capparelli and F. García Einschlag are members of CONICET. L. Carlos thanks the CONICET for a grant supporting his Ph.D. thesis.

Appendix A. Supplementary data

Supplementary data associated with this article can be found, in the online version, at doi:10.1016/j.jphotochem.2008.09.012.

References

[1] M.R.A. Silva, A.G. Trovo, R.F.P. Nogueira, J. Photochem. Photobiol. A: Chem. 191 (2007) 187–192.
[2] G. Sagawe, A. Lehnard, M. Lubber, D. Bahnemann, Helv. Chim. Acta 84 (2001) 3742–3759.
[3] S. Malato, J. Blanco, A. Vidal, D. Alarcon, M.I. Maldonado, J. Caceres, W. Gernjak, Solar Energy 75 (2003) 329–336.
[4] D. Robert, S. Malato, Sci. Total Environ. 291 (2002) 85–97.
[5] I.R. Bautitz, R.F.P. Nogueira, J. Photochem. Photobiol. A: Chem. 187 (2007) 33–39.
[6] D. Bahnemann, Solar Energy 77 (2004) 445–459.
[7] M. Perez-Moya, M. Graells, L.J. del Valle, E. Centelles, H.D. Mansilla, Catal. Today 124 (2007) 163–171.
[8] V. Kavitha, K. Palanivelu, J. Photochem. Photobiol. A: Chem. 170 (2005) 83–95.
[9] O.A. O'Connor, L.Y. Young, Environ. Toxicol. Chem. 8 (1989) 853–862.
[10] M. Rodríguez, A. Kirchner, S. Contreras, E. Chamarro, S. Esplugas, J. Photochem. Photobiol. A: Chem. 133 (2000) 123–127.
[11] M. Rodriguez, V. Timokhin, F. Michl, S. Contreras, J. Gimenez, S. Esplugas, Catal. Today 76 (2002) 291–300.
[12] F. Al Momani, J. Photochem. Photobiol. A: Chem. 179 (2006) 184–192.
[13] A. Goi, M. Trapido, Chemosphere 46 (2002) 913–922.
[14] R. Chen, J.J. Pignatello, Environ. Sci. Technol. 31 (1997) 2399–2406.
[15] Y. Du, M. Zhou, L. Lei, J. Hazard. Mater. 136 (2006) 859–865.
[16] D. Nichela, L. Carlos, F.G. Einschlag, Appl. Catal. B: Environ. 82 (2008) 11–18.
[17] L. Carlos, D. Fabbri, A.L. Capparelli, A. Bianco Prevot, E. Pramauro, F. García Einschlag, Chemosphere 72 (2008) 952–958.
[18] J.E. Frew, P. Jones, G. Scholes, Anal. Chim. Acta 155 (1983) 139–143.
[19] D. Fabbri, L.S. Villata, A.B. Prevot, A.L. Capparelli, E. Pramauro, J. Photochem. Photobiol. A: Chem. 180 (2006) 157–164.
[20] J.J. Pignatello, Environ. Sci. Technol. 26 (1992) 944–951.
[21] R. Chen, J.J. Pignatello, J. Adv. Oxid. Technol. 4 (1999) 447–453.
[22] F. Chen, W. Ma, J. He, J. Zhao, J. Phys. Chem. A 106 (2002) 9485–9490.
[23] S. Scott, Oscillations, Waves, and Chaos in Chemical Kinetics, Oxford University Press, New York, 1994.
[24] F.S. García Einschlag, L. Carlos, A.L. Capparelli, A.M. Braun, E. Oliveros, Photochem. Photobiol. Sci. 1 (2002) 520–525.
[25] A. Santos, P. Yustos, A. Quintanilla, F. García-Ochoa, J.A. Casas, J.J. Rodriguez, Environ. Sci. Technol. 38 (2004) 133–138.
[26] A. Safarzadeh-Amiri, J.R. Bolton, S.R. Cater, Water Res. 31 (1997) 787–798.
[27] D.L. Sedlak, J. Hoigne, Atmos. Environ. 27 (1993) 2173–2185.
[28] J.J. Pignatello, E. Oliveros, A. MacKay, Crit. Rev. Environ. Sci. Technol. 36 (2006) 1–84.
[29] G. Persoone, B. Marsalek, I. Blinova, A. Torokne, D. Zarina, L. Manusadzianas, G. Nalecz-Jawecki, L. Tofan, N. Stepanova, L. Tothova, B. Kolar, Environ. Toxicol. 18 (2003) 395–402.